


 Cite this: *RSC Adv.*, 2023, 13, 506

Catalyst-free synthesis of low-temperature thermally actuated shape memory polyurethanes with modified biobased plasticizers

 Basharat Ali,^a Muhammad Atif,^b *^a Muhammad Perviaz,^b Adnan Irshad,^a Muhammad Abdullah^a and Muhammad Ahmad Mobeen^a

Recent years have seen research into developing specific application-based materials with particular components. Bio-based polyurethanes (PUs) with self-tightening effect through shape recovery at low temperature have been designed from sesame oil-based plasticizer (HSSO). Without using a catalyst, the produced plasticizer was used to create PU samples. In contrast, orcein-based PU has been created both with and without HSSO. The prepared samples have been analyzed through instrumental as well as chemical analyses for surface chemistry, thermal stability and morphology. The gel content and water absorption capacity of HSSO based PU samples has been observed to be 99.27% and 14.94%, respectively. Shape memory study of the PU samples revealed that HSSO-based PU showed fast shape recovery at 60 °C with shape recovery rate (R_r) and shape fixing rate (R_f) of 94.44% and 5%, respectively, in 150 seconds, whereas at 36 °C the sample showed 85% R_r in 15 minutes with 93.1196 N force and 52.78% R_r without force. Low-temperature thermal actuation and high water uptake highlight the prepared samples as suitable candidates for self-tightening structures in textile and biomedical fields.

 Received 30th October 2022
 Accepted 13th December 2022

DOI: 10.1039/d2ra06862a

rsc.li/rsc-advances

1 Introduction

Stimulus-responsive restoration of a polymeric material to its original shape after specific deformation has opened a new dimension in material applications.¹ These stimuli include, but are not limited to, changes in temperature,² light,³ electricity,⁴ pH,⁵ and other similar variables. Biomedical devices such as cardiovascular stents,⁶ sutures,⁷ drug-eluting stents⁸ and clot removal devices,⁹ and tissue engineering,¹⁰ have made extensive use of SMPs due to their biocompatibility,¹¹ biodegradability,¹¹ and human body temperature shape recovery.^{12–14} With their tunable transition temperatures for shape recovery and high levels of biocompatibility, shape memory polyurethanes (SMPUs) have shown great promise as responsive materials for use in biomedical devices inside the human body,^{12–14} accompanied by coating material, packing materials and smart textile.^{15–17}

However, environmental concerns and exhausted petroleum reserves have shifted the focus to SMPUs with biobased origin rather than petrochemical origin.¹⁸ Currently, vegetable oils like soyabean oil,¹⁹ castor oil,²⁰ sunflower oil,²¹ jatropha oil²² and palm kernel oil,²³ are the most common source for bio-based

SMPUs (bio-SMPUs), but slow curing,²⁴ catalytic constraint^{25,26} and reduced elastic strength^{27–29} has limited their applications in comparison to petrochemical based SMPUs. This is because the micro-phase separation of PU is negatively impacted by the lengthy dangling chains present in vegetable oil polyols (PUs). Researchers have tried to control the length of side chains either by bio-based polyester diols,²⁴ or by rosin-based chain extender³⁰ but found not ideal for biological applications due to their shape recovery below body temperature. PU based polyurethane SMPs had ability to recover its shape to maximum degree but different chain extenders and catalyst were applied to control their elastic properties^{25,31,32} as shown in Table 6. Considering these limitations, ecofriendly SMPUs, with recyclable nature but high mechanical strength, have always been in dire need.

In this research, modified sesame oil-based polyols have been utilized to formulate SMPUs, without any chain extender or catalyst, but with quick shape recovery at very low thermal actuation. Two step treatment *i.e.* epoxidation and hydroxylation, has been performed to obtain suitable polyol as plasticizer for shape memory property.

2 Materials and method

2.1 Materials

Sesame seed oil (SSO) extracted from sesame seed at commercial extracting unit, hydrogen peroxide (35%, Sigma-Aldrich), formic acid (DAEJUNG Chemicals & Metals), glacial acetic acid

^aChemistry Department, University of Education Lahore, Vehari Campus, Officers' Colony, Vehari-61100, Punjab, Pakistan. E-mail: chemistatif@yahoo.com; muhammad.atif@ue.edu.pk; Tel: +92-3024757979

^bDepartment of Basic & Applied Chemistry, Faculty of Science & Technology, University of Central Punjab, Lahore, Pakistan



(100% pure, Merck KGaA), orcein reagent (Sigma-Aldrich), pure ethyl alcohol (Sigma-Aldrich), toluene 2,4-diisocyanate (TDI, extra pure, DAEJUNG Chemicals & Metals), benzene (Sigma-Aldrich), paraffin oil (Sigma-Aldrich) were utilized as raw materials in this practical work.

2.2 Method

2.2.1 Epoxidation of SSO (ESSO). A mixture of acetic acid (0.73 moles) and 35% hydrogen peroxide (2.35 moles) was refluxed at 40 °C for 15 minutes, SSO (0.08 moles) was added dropwise while stirring and refluxing (40 °C). After complete addition of SSO, refluxing was continued for 2.5 hours at 40 °C and 30 minutes at 130 °C. Then reaction mixture was allowed to cool at room temperature. The upper layer with bright yellow colour was separated and placed in desiccator for 6 hours. The final product (ESSO) was obtained with 90.22% yield.

2.2.2 Hydroxylation of ESSO (HSSO). A mixture of ethanol (0.804 moles), deionized water (1.66 moles) and 30 ml organic acids (acetic acid : formic acid by vol. 1 : 1) was heated at 65 °C with vigorous stirring (1500 rpm). ESSO (0.022 moles) was added dropwise and refluxed, while stirring, for 30 minutes at 65 °C. Then reaction mixture was allowed to cool at r.t. HSSO layer (lower layer) was separated from aqueous layer and placed in desiccator for 6 hours. 90% yield of HSSO (pale-yellow color) was obtained.

2.2.3 Preparation of HSSO-PU. HSSO (0.0074 moles) was heated at 60 °C, while stirring (650 rpm), for 5 minutes, and TDI (0.028 moles) was added dropwise while vigorously stirring at 60 °C to avoid bubbling. The mixture was heated for 10 minutes while vigorously stirring. Viscous dispersion was then shifted into mold and set to dry for 72 hours at room temperature. Very light-yellow thin layer of HSSO-based PU about 1 mm thickness was obtained. Proposed reaction scheme is presented in Scheme 1.

2.2.4 Preparation of Or-PU. Orcein (0.0004 moles) was dissolved with stirring in ethanol (0.338 moles) at r.t. and heated at 60 °C for 5 min. Then TDI (0.0417 moles) was added

dropwise in 2 min and heated while stirring at 60 °C for 10 minutes. The viscous dark red material was shifted into plastic mold and allowed to cure for 72 hours. Or-PU with 1 mm thickness was obtained. Proposed reaction scheme is presented in Scheme 1.

2.2.5 Preparation of Or-HSSO-PU. Orcein (0.0004 moles) ethanol (0.338 moles) solution was mixed with HSSO (0.00165 moles) and stirred for 5 min. Then TDI (0.0556 moles) was added dropwise (in 3 minutes) with stirring and heating at 60 °C for 10 minutes. The dark reddish viscous liquid was shifted into mold and set to dry for 72 hours. Or-HSSO-PU with thickness of 1 mm was obtained. Proposed reaction scheme is presented in Scheme 1.

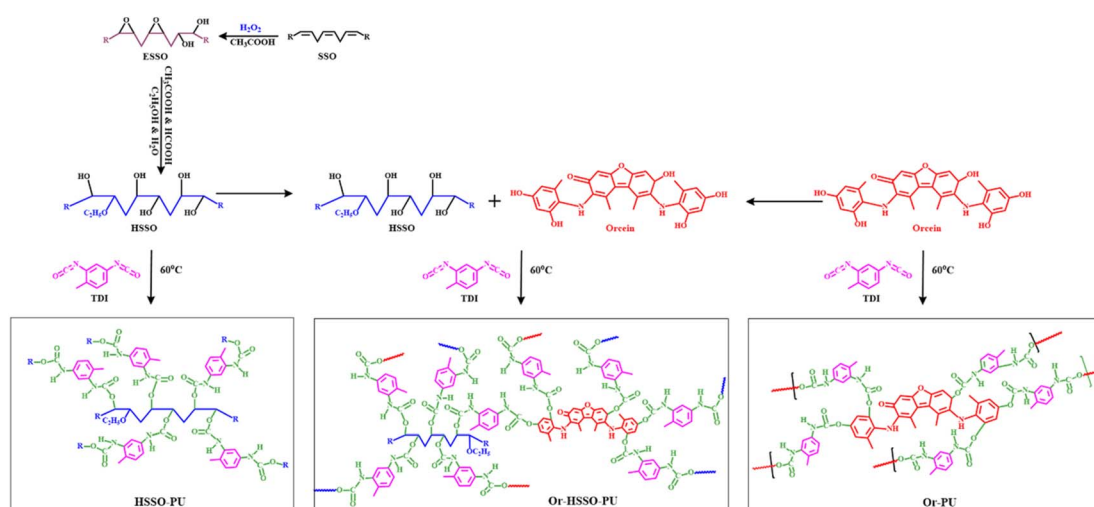
3 Characterizations

Synthesized PU samples have been analyzed through FTIR (IRSpirit) Shimadzu with diamond ATR in range 500–4000 cm^{-1} , TGA/DSC (STA SKZ1060A Industrial Co., Limited) from room temperature to 500 °C at ramp rate of 10 °C min^{-1} for 5 mg sample in Al crucible using oxidative environment and air as purge gas, light microscope (IRMECO GmbH & Co., IM-910). The morphology and surface roughness of synthesized PU composites have been studied by scanning electron microscope (SEM, ZEISS EVO, Carl Zeiss) and atomic force microscopy (AFM). Molar mass of treated SSO was determined by ebullioscopic method (eqn (1)) taking benzene as solvent.

$$\Delta T_b = K_b m \quad (1)$$

where ΔT_b = elevation in boiling point of specific solvent, K_b = ebullioscopic boiling constant of specific solvent and m = molality of unknown sample. For benzene, the value of ebullioscopic boiling constant is 2.53 °C kg mol^{-1} .³³

Iodine value (IV) was determined by reported method.³⁴ 0.2 g sample with 10 ml chloroform was stirred with 30 ml of Hanus solution for 15 minutes. 10 ml of 15% KI and 100 ml DI water



Scheme 1 Synthesis of HSSO-PU, Or-HSSO-PU and Or-PU.



were added and titrated against 0.1 N $\text{Na}_2\text{S}_2\text{O}_3$ till yellow colour, added 2–3 drops of starch indicator and titrated again till blue colour. Calculated IV by using eqn (2).

$$\text{IV} = \frac{(B - S) \times N \text{ of } \text{Na}_2\text{S}_2\text{O}_3 \times 0.127 \text{ g meq.}^{-1} \times 100}{\text{weight of sample (g)}} \quad (2)$$

where B and S are the volume used of $\text{Na}_2\text{S}_2\text{O}_3$ against blank solution and sample and N is the normality of $\text{Na}_2\text{S}_2\text{O}_3$.

Epoxy value (EV) was determined by HCl-acetone titration method.³⁵ 0.25 g sample was stirred in 5 ml HCl (0.1 N) and 35 ml of acetone. 5 ml mixture, with 2–3 drops of indicator, was titrated against 0.1 N NaOH till pink color. EV value was calculated by eqn (3).

$$\text{EV} = \frac{(B - S) \times N \text{ of HCl}}{W \times 10} \quad (3)$$

where S and B are the volume used of NaOH against sample and blank solution, and W is the weight of sample.

Samples' density was determined by using mass/volume relationship.³⁶ Gel contents were measured by a method reported in literature.³⁷ Calculated amount of PU samples (HSSO-PU, Or-HSSO-PU and Or-PU) was soaked in 20 ml of dichloromethane (DCM) for 24 hours. Then samples were removed from solvent and dried at 40 °C, and weighted to calculate gel contents by using eqn (4) and (5).

$$\% \text{ extract} = \frac{W_s - W_d}{W_0} \times 100 \quad (4)$$

$$\% \text{ gel content} = 100 - \% \text{ extract} \quad (5)$$

where W_s is weight of sample and W_d is weight of dried sample.

Water absorption capacity was determined by a method reported in literature.³⁸ Weighed PU samples were dipped in deionized water for 48 hours. At regular time intervals samples were removed from water, dried and weighed to determine water absorption by eqn (6).¹⁵

$$\text{Water absorption capacity}(\%) = \frac{W_t - W_0}{W_0} \times 100 \quad (6)$$

where W_t = weight of sample after dipping, W_0 = weight of dried sample.

Hemolytic activity, antioxidant activity and antibacterial activity of synthesized PU composites have been determined by reported methods^{39–41} using eqn (7) and (8), respectively.

$$\% \text{ homolysis} = \frac{A_t - A_n}{A_c - A_n} \times 100 \quad (7)$$

where A_t is the absorbance of the test sample. A_n is the absorbance of the control (saline control) A_c is the absorbance of the control (Triton control).

$$\text{Antioxidant activity} = \frac{A_{\text{blank}} - A_{\text{sample}}}{A_{\text{blank}}} \times 100 \quad (8)$$

where; A_{blank} is the absorbance of the control reaction (containing all reagents except the extract) and A_{sample} is the absorbance of the mixture containing the extract.

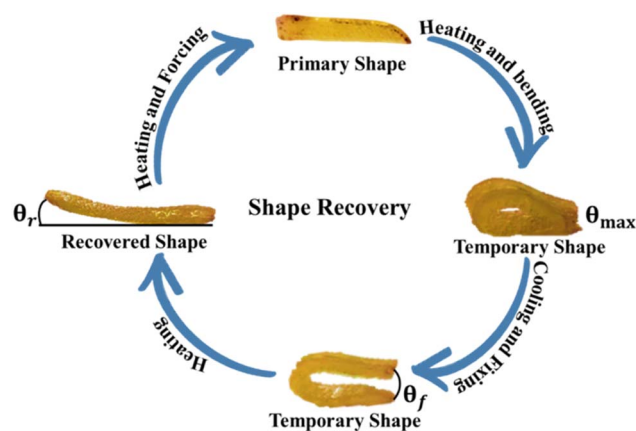


Fig. 1 Shape memory bending test.

3.1 Shape memory test

Rectangular strips of PU films having dimension 3 cm × 6 mm × 3 mm (Fig. 1) were used to study shape memory behavior (Fig. 1).

For shape memory study, films were heated at 54 °C, bent and cooled to maintain temporary shape. Thermal stimulus (50–60 °C) was provided to films for restoration of original shape. The displacement of shape from θ_{max} while cooling and fixing is known as angle of fixity (θ_f). Attained position by bent film while displacing towards original shape after heating is known as recovered shape and the difference of angle from starting position is known as angle of recovery (θ_r). Cycles of conversion original → temporary → original shape were repeated five times. Ability of PU films to gain temporary shape and restoration to original shape under the influence of temperature is the shape recovery rate (R_r) and shape fixity rate (R_f), calculated with eqn (9) and (10).¹⁵

$$R_f (\%) = \frac{180 - \theta_f}{180} \times 100 \quad (9)$$

$$R_r (\%) = \frac{180 - \theta_r}{180} \times 100 \quad (10)$$

4 Results and discussions

4.1 Physico-chemical analyses

Molecular mass (MM), iodine value (IV), epoxy value (EV) and density of unmodified and modified SSO were calculated to confirm the effectiveness of modification protocol. Upsurge in

Table 1 Characteristic data of samples

Sample ID	MM (g mol ⁻¹)	IV	EV	Density (g cm ⁻³)
SSO	1103.8	129.19	104.76	0.9130
ESSO	1290.3	114.20	131.10	0.9523
HSSO	1322.6	100.66	104.90	1.0889



MM and density of modified samples in comparison to unmodified sample, confirmed the change in molecular assembly. IV difference signposted the effective consumption of unsaturated contents during two step modification. EV counter-confirmed the effectiveness of two-step modification protocol (*i.e.* epoxidation and hydroxylation) (Table 1).

4.2 FTIR analyses

SSO to ESSO modification was studied by FTIR data (Fig. 2). SSO spectra showed peaks of different functional groups (*e.g.* C=C, C-O-C and =C-H) at 723 cm^{-1} , 1242 cm^{-1} and 3008 cm^{-1} respectively.^{42,43} After treatment, ESSO spectra showed a reduction in C=C peak with peak area condensed thrice, whereas, absorbance peak of C-O-C became sharp and wide with peak area almost doubled. At the same time, epoxy peak with peak area 0.62 was observed at 826 cm^{-1} in ESSO spectral line.⁴² Disappearance of =C-H peak (3008 cm^{-1})⁴³ in ESSO, may be attributed to conversion of alkene into epoxy, confirmed by the appearance of epoxy peak in ESSO. The peaks present at 2347 cm^{-1} and 1738 cm^{-1} represent carbonyl functional group.⁴³ FTIR spectra of HSSO (Fig. 2) obtained after treating ESSO with organic acids (acetic acid and formic acid) in ethanol and water, showed a reduction in C-O-C peak at 1242 cm^{-1} and also in epoxy peak at 826 cm^{-1} . Moreover, -OH peak appeared at 3502 cm^{-1} .⁴³ The conformation of OH induction may be done with C-O peak formation at 1037 cm^{-1} .⁴³

HSSO, as biobased diol, upon reaction with TDI resulted in HSSO-PU (Fig. 3). Peaks at 3502 cm^{-1} and 2245 cm^{-1} in HSSO FTIR spectra, represent OH in HSSO and NCO in TDI, respectively.³³ Upon reaction of HSSO with TDI, disappearance of both OH and NCO peaks in product (Fig. 3) confirmed the consumption of these functional groups along with the formation of a new functional group C-O at 1054 cm^{-1} .⁴³ Breakdown of C=N bond in TDI, resulted in new bonds, *i.e.* C-N with peak at 1219 cm^{-1} ,³³ N-H with peak at 3333 cm^{-1} ,³³ and carbonyl with peak at 1738 cm^{-1} .⁴³ Peak at 1533 cm^{-1} indicated the presence of cyclic alkenes.³³

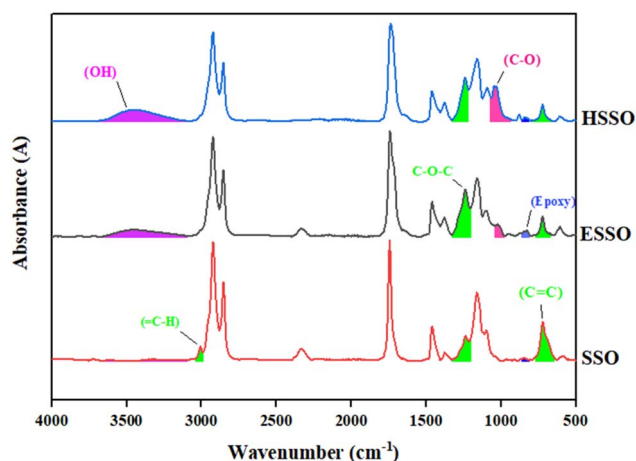


Fig. 2 FTIR of SSO, ESSO and HSSO.

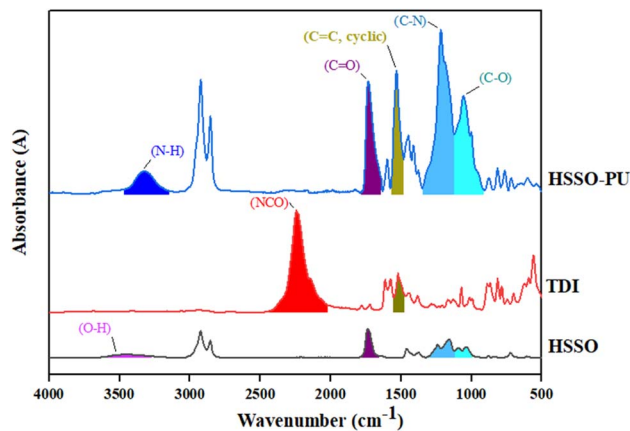


Fig. 3 FTIR of HSSO-PU and its reactants.

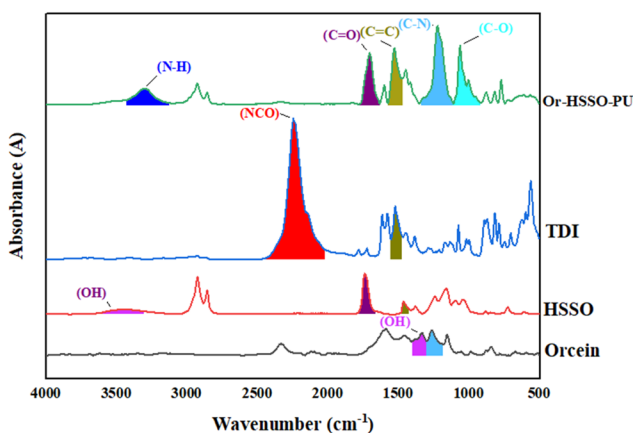


Fig. 4 FTIR of Or-HSSO-PU and its reactants.

Or-HSSO-PU sample along with ingredients was analyzed through FTIR (Fig. 4). Peaks of NCO and OH were found at 2245 cm^{-1} and 1328 cm^{-1} , respectively,^{15,33} while HSSO hydroxyl group was observed at 3502 cm^{-1} .³³ After reaction of orcein and HSSO with TDI, both NCO and OH peaks disappeared rising new peaks in product. It is assumed that polyols OH reacted with C=N in TDI, resulting in CO bond between TDI and polyol with peak at 1054 cm^{-1} .⁴³ Similarly, N linked with H and peak appeared at 3299 cm^{-1} .¹⁵ Likewise, breakup of double bond between C and N resulted in single bond left with peak at 1219 cm^{-1} .^{15,33,43} Carbonyl peak at 1703 cm^{-1} , also increased in size. The peak of cyclic C=C appeared at 1533 cm^{-1} .

Similarly, FTIR analysis was applied on Or-PU and its reactants to observe different functional group formed (Fig. 5). Phenolic OH group was observed at 1328 cm^{-1} . After reaction between polyol and isocyanate, NCO and OH functionalities disappeared with new group formation in product, *i.e.* N-C, C-O and N-H. Peaks of NCO and OH were at 2254 cm^{-1} and 1328 cm^{-1} respectively.^{15,33,43} Appearance of these new peaks in Or-PU confirmed the synthesis of product as shown in Fig. 5.



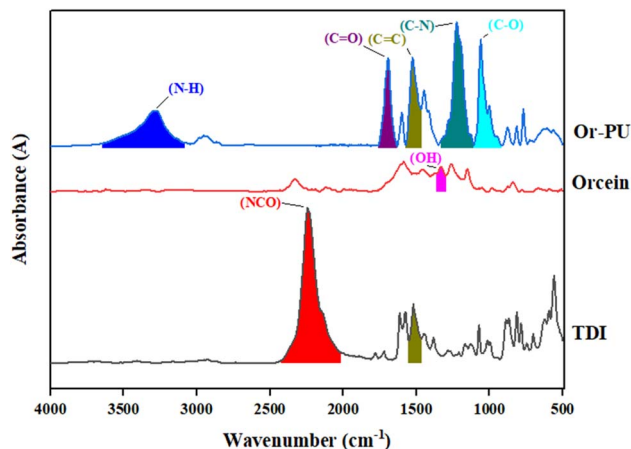


Fig. 5 FTIR analysis of Or-PU and its reactants.

4.3 TGA

Thermal stability of prepared samples has been studied with TGA (Fig. 6). Data revealed that incorporation of orcein imparts thermal instability into samples, which might be attributed to higher oxidizable contents on its surface. Thermal degradation of sample prepared from biobased material was observed least in first two segments, which might be attributed to least oxidizable contents on its surface. In third segment (above 400 °C) thermal stability pattern reversed *i.e.* biobased polyol containing PU degraded quickly in comparison to samples having orcein as polyol. This reversal in degradation pattern may be attributed to fact that orcein based PU samples lost most of oxidizable components in first two segments and became thermally stable whereas biobased polyol containing PU, at 450 °C (Fig. 6), decomposed carbon chains into smaller fragments, prone to thermal degradation.⁴⁴

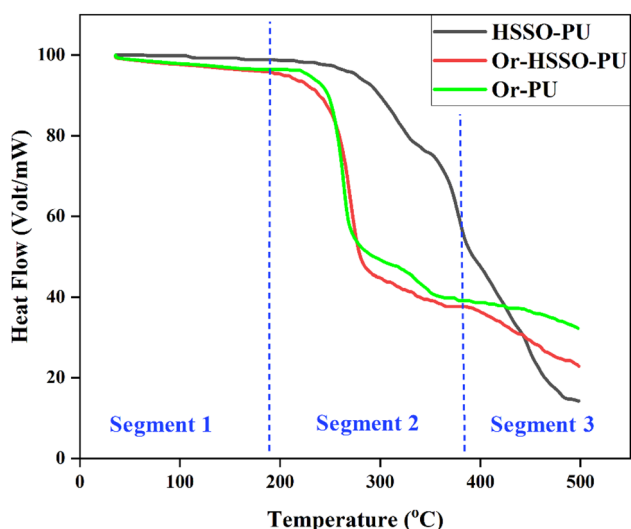


Fig. 6 TGA of PU composites.

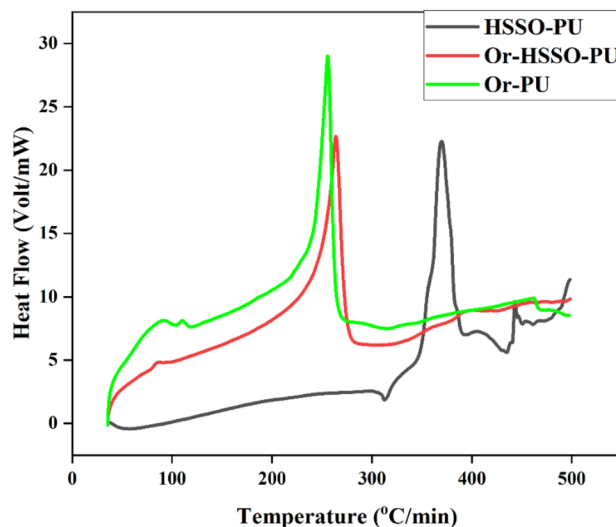


Fig. 7 DSC of PU composites.

Table 2 DSC data of prepared PU samples

Sample ID	$T_{g,HS}$ (°C)	Thermal melt	
		Temperature (°C)	ΔH_m (cal.)
HSSO-PU	322.8	369.6	132.5
Or-HSSO-PU	88.6	264.4	136.4
Or-PU	90.4	255.6	141.9

4.4 DSC

Prepared PU samples were analyzed through DSC (Fig. 7, Table 2). Comparative analysis, on the basis of increasing biobased polyol component, showed an augmentation trend in T_g of hard segment (TDI), signposting micro-phasic separation of hard and soft segments of PU samples by adding HSSO.⁴⁵ About 100 °C increase in thermal melt of HSSO-PU than Or-PU is due to its well-defined microcrystalline structure which signpost increased cross linking density of rubbery soft segments (polyols), moreover 10 cal. low ΔH_m of HSSO-PU than Or-PU represents less thermal dissipation of amorphous HSSO.⁴⁶ This data evidenced a vivid micro-phasic level separation of hard and soft segments in HSSO-PU.

Thermal melt enthalpy increases with increasing polyol content in PU structure.⁴⁵ Or-PU showed highest ΔH_m of all samples indicating highest alcoholic content involvement in polymerization, which might be attributed to condensed structure of orcein, but high thermal dissipation capacity of orcein decreased thermal melt temperature of Or-PU than HSSO-PU.

4.5 Gel content & water absorption capacity

Gel content analysis was applied on prepared PU samples (Table 3). HSSO-PU was found to have the highest gel contents (99.27%) in comparison to Or-PU (98.32%) and Or-HSSO-PU



Table 3 Gel content (%) and water absorption capacity (%) of PU samples

Samples	Gel content (%)	Water absorption capacity (%)						
		0 h	1 h	2 h	3 h	4 h	24 h	48 h
HSSO-PU	99.27	0	3.9	4.09	4.09	9.42	9.71	14.94
Or-HSSO-PU	97.66	0	0.47	1.42	4.42	3.63 ^a	7.4 ^a	5.53 ^a
Or-PU	98.32	0	3.14	5.45	6.7	7.54	10.06	15.01

^a Dissolution was observed for a small portion of sample.

(97.66%) verifying huge quantity of constituents to be cross-linked during synthesis of PU samples.

Water absorption capacity of prepared PU samples was also studied to confirm their hydrophilic nature and biodegradation behavior. Water absorption results (Table 3) indicated an upsurge with temperature rise, which links soft segment's interaction with water. Swelling of material relates inversely with crosslinking density of the constituents, *i.e.* Or-PU composite had high swelling proportion as compared to HSSO-PU composite due to low crosslinking density.

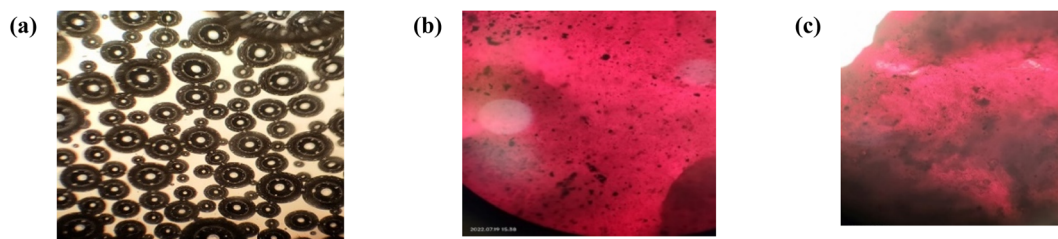


Fig. 8 Microscopic images of (a) HSSO-PU (b) Or-HSSO-PU (c) Or-PU.

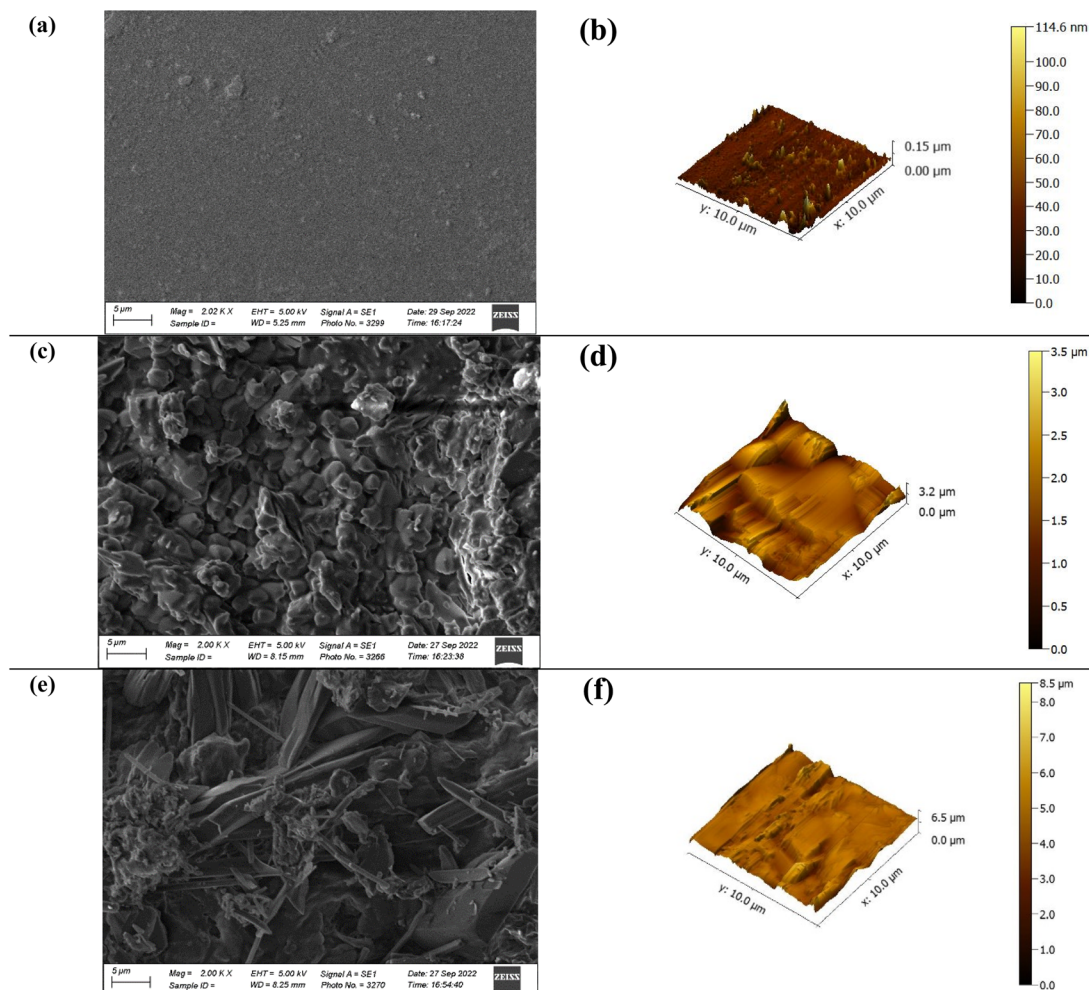


Fig. 9 SEM and AFM diagrams of (a and b) HSSO-PU, (c and d) Or-HSSO-PU, (e and f) Or-PU.



Table 4 Toxicity of PU composites at different concentrations

Concentration (mg ml ⁻¹)	Toxicity				Antioxidant activity			
	HSSO-PU	Or-HSSO-PU	Or-PU	Triton X-100	HSSO-PU	Or-HSSO-PU	Or-PU	Ascorbic acid
12	12.3 ± 0.17	13.2 ± 0.11	14.2 ± 0.14	97.5 ± 1.8	75.34 ± 0.79	74.5 ± 0.77	69.22 ± 0.69	95.93 ± 1.5
6	10 ± 0.1	10.8 ± 0.09	11.4 ± 0.09		71.72 ± 0.7	70.1 ± 0.71	66.43 ± 0.58	90.62 ± 1.1
3	7.9 ± 0.08	8.7 ± 0.06	9.1 ± 0.07		63.09 ± 0.61	68.4 ± 0.66	55.57 ± 0.51	88.71 ± 0.99
1.5	3.8 ± 0.05	4.6 ± 0.06	7.8 ± 0.04		55.84 ± 0.48	65.6 ± 0.55	54.03 ± 0.43	85.22 ± 0.83
0.75	1.8 ± 0.03	2.8 ± 0.02	3.7 ± 0.03		53.06 ± 0.4	63.3 ± 0.51	46.23 ± 0.33	80.29 ± 0.78

4.6 Morphology

Microscopic images of HSSO-PU, Or-HSSO-PU and Or-PU (Fig. 8) presented segmental separation of soft and hard

components in HSSO-PU, whereas Or-PU showed a homogeneous dispersion of orcein throughout PU sample. Segmental separation type configuration in HSSO-PU has been supported

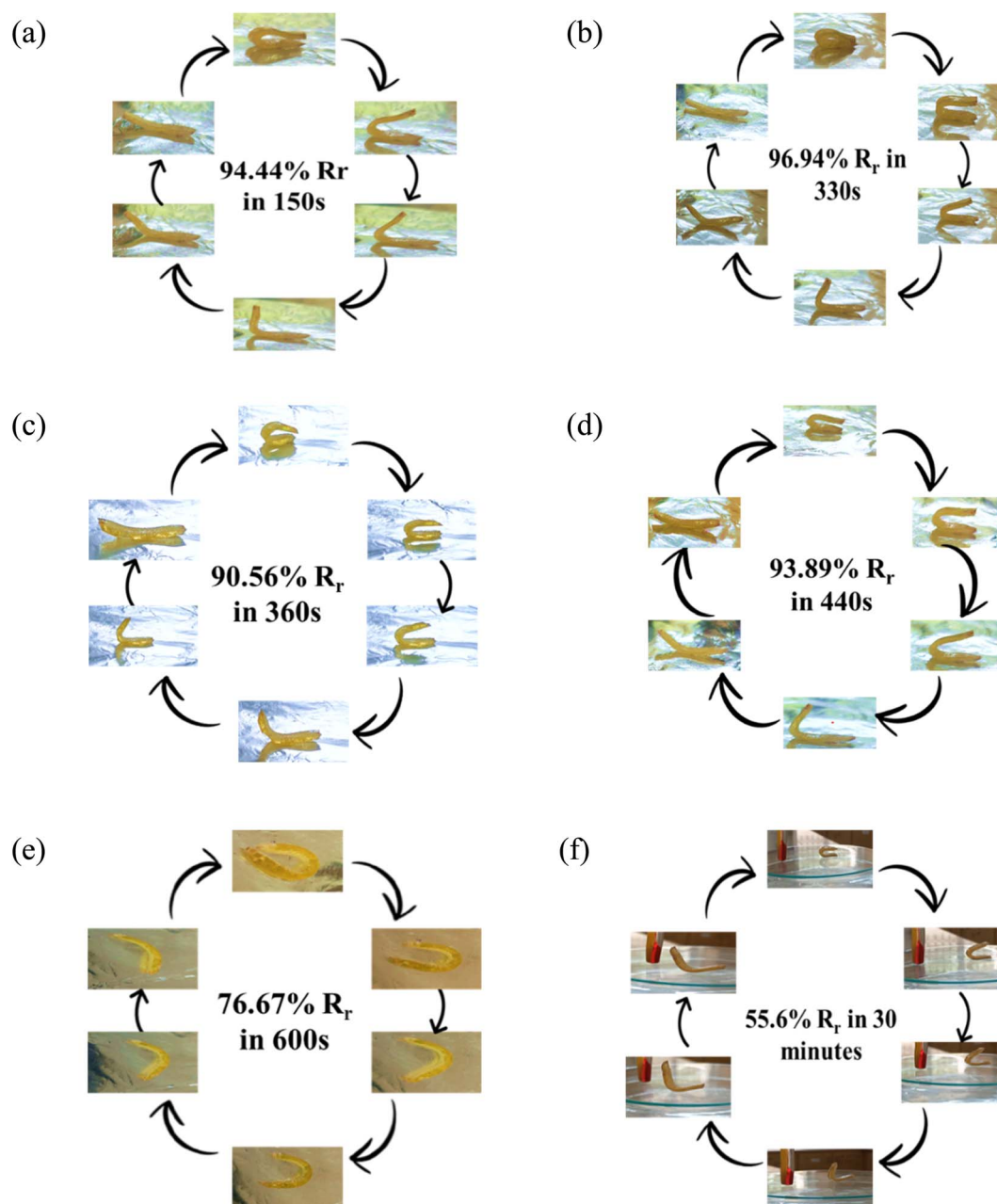


Fig. 10 Shape memory study of HSSO-PU at (a) 60 °C, (b) 55 °C, (c) 54 °C, (d) 52 °C, (e) 51 °C, (f) 40 °C.



Table 5 Shape recovery behavior of HSSO-PU at different temperatures

Sample ID	Temperature (°C)	Recovery time (s)	Shape recovery rate% (R_r)	Ref.
HSSO-PU	60	150	94.44	This work
	55	330	96.94	
	54	360	90.56	
	52	440	93.89	
	51	600	76.67	
	40	30 min	55.6	
SMPUs	35–45	NR	98	47
PU/PEEAMA	60	5	96	48

by DSC thermal melt data, which specified well-defined microcrystalline hard segments.

4.7 SEM and AFM

SEM and AFM analyses of prepared samples (Fig. 9) at μ level revealed homogeneity and smoothness in sample with biobased plasticizer (HSSO). On the contrary, orcein amalgamation imparted non-homogeneity and surface roughness (almost 40 folds to biobased plasticizer), which might be considered for the structural damage during shape memory studies.

4.8 Bioactivities

Hemolytic activity showed mild toxicity at 12 mg ml^{-1} concentration, which shrank with concentration drop (Table 4). The highest was shown by Or-PU at 14.2 ± 0.14 while the lowest was by HSSO-PU at 12.3 ± 0.17 at 12 mg ml^{-1} concentration. Likewise, antioxidant potential of HSSO-PU has been observed at a high antioxidant value of 75.34 ± 0.79 followed by Or-HSSO-PU and Or-PU that is 74.5 ± 0.77 and 69.22 ± 0.69 , respectively.

4.9 Antibacterial activity

Antibacterial activity of samples showed that *E. coli* is sensitive bacteria against samples that show maximum zone of inhibition in HSSO-PU and Or-PU, while *B. subtilis* and *S. aureus* also show a zone of inhibition against HSSO-PU and Or-HSSO-PU. The antibacterial activity of HSSO-PU, Or-HSSO-PU, and Or-PU at sample concentration of 12 mg ml^{-1} was observed to be 1.8, 1.1, 1.1 for *E. coli*, 2.8, 1.7 and 1.7 for *B. subtilis* and 1.9, 2.4 and 1 for *S. aureus*, respectively. For 6 mg ml^{-1} sample concentration, the antibacterial activities of HSSO-PU, Or-HSSO-PU, and Or-PU were 1.1, 0 and 0.5 for *E. coli*, 2, 0 and 1.2 for *B. subtilis*, and 1.2, 0 and 0 for *S. aureus*, respectively. While

HSSO-PU exhibits bacterial resistance behaviour with 0.7, 0.5, and 0.3 antibacterial activity for *E. coli* for lower sample concentrations (3, 2.5, and 0.75 mg ml^{-1}). However, other samples with lower sample concentrations failed to exhibit antibacterial efficacy against referred bacterial species.

4.10 Shape memory

Shape memory of PU samples (HSSO-PU, Or-HSSO-PU and Or-PU) was studied under different temperatures (Fig. 10). Or-HSSO-PU and Or-PU showed rigidity till 40°C and broke but above 40°C started melting and did not show any shape recovery behavior. This may be attributed to strong thermal dissipation behavior of orcein, which caused melting of sample at a specific temperature through structural damage. On the other side, HSSO-PU started showing flexibility at 50°C . Shape memory and shape fixing behaviors of HSSO-PU films were studied in temperature range of $50\text{--}60^\circ\text{C}$ (Table 5). Fast shape recovery was found with temperature rise but with more shape fixing, which may be attributed to structural damages of HSSO-PU at 60°C (Fig. 11).

Biodegradability and water uptake response of PU samples containing HSSO (Table 3) has widened the application scope of these materials in textile as well as biomedical not only as drug carrier but also as shape recovery materials. To recognize shape memory response of HSSO-PU at human body temperature,

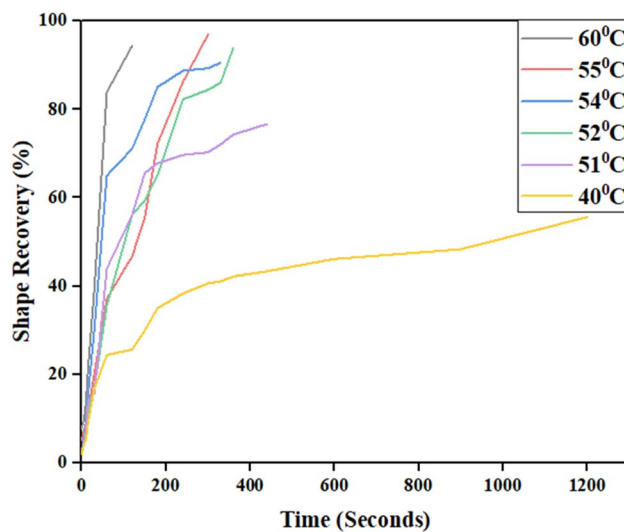


Fig. 11 Shape recovery graph of HSSO-PU composite at different temperatures.

Table 6 Composition and R_r time comparison of body temperature sensitive PU

Sr. no.	Polyol	Isocyanate	Catalyst	Chain extender	R_r time (seconds)	Ref.
1	Co-PLAols	IPDI	SnOct ₂	BDO, HDO, EG	60	25
2	PCL diol	MDI-50	SnOct ₂	N/R	15	31
3	Co-PLA tetraol	HDI	SnOct ₂	PETP	101	32
4	HSSO	TDI	N/A	N/A	30 min	This work



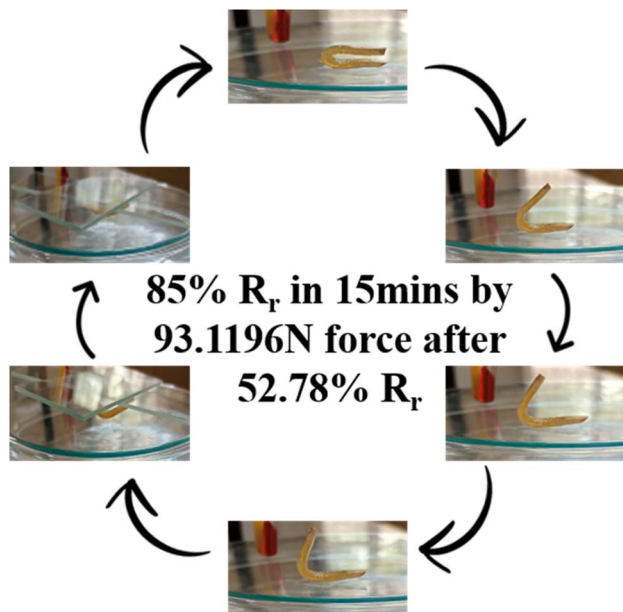


Fig. 12 Shape memory study of HSSO-PU at 36 °C.

shape recovery at 36 °C was studied (Fig. 12). 52.78% shape recovery was found without any force whereas 85% shape recovery was observed at 93.1196 N force.

Upon comparison of shape recovery data from already published works, it is being claimed that current research has neither used any types of chain extenders nor catalyst to support shape recovery rate at body temperature, furthermore, not any specially designed commercial product to impart flexibility (MDI-50) has been incorporated in molecular design. This outcome *i.e.* synthesis without special chemical, will support HSSO-PU's expanded biomedical application domain.

5 Conclusion

In this research biobased polyols have been designed through an eco-friendly and facile approach. SSO has been treated to obtain hydroxylated plasticizer (HSSO), which has induced low thermal actuation shape recovery with high thermal stability in PU samples, whereas orcein has imparted rigidity and easy thermal degradation. HSSO has framed separate and well-defined hard and soft segments in PU. Prepared samples have 100% thermal stability till 270 °C, but shape recovery response initiated at very low thermal stimulus *i.e.* 36 °C, which has made it a suitable candidate for self-tightening structures not only in textiles and biomedical applications like dental implants, but also in all applications that require shape recovery at very low temperature.

Conflicts of interest

There are no conflicts to declare.

References

- 1 W. M. Huang and et al, ., Shape memory materials, *Mater. Today*, 2010, **13**(7), 54–61.
- 2 C. Liu and et al, ., Magnetic mesoporous silica microspheres with thermo-sensitive polymer shell for controlled drug release, *J. Mater. Chem.*, 2009, **19**(27), 4764–4770.
- 3 P. Pan and et al, ., Photosensitive drug delivery systems for cancer therapy: Mechanisms and applications, *J. Controlled Release*, 2021, **338**, 446–461.
- 4 M. Gosecka and M. Gosecki, Chemoresponsive polymer systems for selective molecular recognition of organic molecules in biological systems, *Acta Biomater.*, 2020, **116**, 32–66.
- 5 F. Ofridam and et al, ., pH-sensitive polymers: Classification and some fine potential applications, *Polym. Adv. Technol.*, 2021, **32**(4), 1455–1484.
- 6 Y. Li and et al, ., 4D printed shape memory polymers and their structures for biomedical applications, *Sci. China: Technol. Sci.*, 2020, **63**(4), 545–560.
- 7 J. Delaey, P. Dubruel and S. Van Vlierberghe, Shape-memory polymers for biomedical applications, *Adv. Funct. Mater.*, 2020, **30**(44), 1909047.
- 8 V. C. Sonawane and et al, ., Fabrication and characterization of shape memory polymers based bioabsorbable biomedical drug eluting stent, *Artif. Cells, Nanomed., Biotechnol.*, 2017, **45**(8), 1740–1750.
- 9 W. Zhao and et al, ., Shape memory polymers and their composites in biomedical applications, *Mater. Sci. Eng., C*, 2019, **97**, 864–883.
- 10 M. Zare and et al, ., Highly porous 3D sponge-like shape memory polymer for tissue engineering application with remote actuation potential, *Compos. Sci. Technol.*, 2019, **184**, 107874.
- 11 X. Cheng and et al, ., Enhanced biocompatibility of polyurethane-type shape memory polymers modified by plasma immersion ion implantation treatment and collagen coating: an *in vivo* study, *Mater. Sci. Eng., C*, 2019, **99**, 863–874.
- 12 D. J. Maitland and et al, ., Photothermal properties of shape memory polymer micro-actuators for treating stroke, *Lasers Surg. Med.*, 2002, **30**(1), 1–11.
- 13 S. Thakur and J. Hu, Polyurethane: a shape memory polymer (SMP), *Aspects of polyurethanes*, 2017, pp. 53–71.
- 14 P. Ping and et al, ., Shape-memory and biocompatibility properties of segmented polyurethanes based on poly (L-lactide), *Frontiers of Chemistry in China*, 2007, **2**(4), 331–336.
- 15 S. S. Khasraghi, A. Shojaei and U. Sundararaj, Bio-based UV curable polyurethane acrylate: Morphology and shape memory behaviors, *Eur. Polym. J.*, 2019, **118**, 514–527.
- 16 A. Lendlein and S. Kelch, Shape-Memory Polymers, *Angew. Chem., Int. Ed.*, 2002, **41**(12), 2034–2057.
- 17 H. Xie, K.-K. Yang and Y.-Z. Wang, Photo-cross-linking: a powerful and versatile strategy to develop shape-memory polymers, *Prog. Polym. Sci.*, 2019, **95**, 32–64.



- 18 H. S. El-Sheshtawy and et al, ., Eco-friendly polyurethane acrylate (PUA)/natural filler-based composite as an antifouling product for marine coating, *Appl. Microbiol. Biotechnol.*, 2021, **105**(18), 7023–7034.
- 19 T. Tsujimoto, T. Takayama and H. Uyama, Biodegradable shape memory polymeric material from epoxidized soybean oil and polycaprolactone, *Polymers*, 2015, **7**(10), 2165–2174.
- 20 J. Lu and et al, ., Self-healable castor oil-based waterborne polyurethane/MXene film with outstanding electromagnetic interference shielding effectiveness and excellent shape memory performance, *J. Colloid Interface Sci.*, 2021, **588**, 164–174.
- 21 S. Nicolas and et al, ., Shape memory epoxy vitrimers based on waste frying sunflower oil, *J. Appl. Polym. Sci.*, 2021, **138**(36), 50904.
- 22 L. L. Taung Mai and et al, ., Non edible oil-based epoxy resins from Jatropha oil and their shape memory behaviors, *Polymers*, 2021, **13**(13), 2177.
- 23 N. Trinh and et al, ., The Effect of Polyol Types and Molecular Weight on the Shape Memory Properties of Palm Kernel Oil-based Polyurethane, *Mater. Today: Proc.*, 2019, **17**, 898–904.
- 24 L. Zhang and et al, ., Bio-based shape memory polyurethanes (Bio-SMPUs) with short side chains in the soft segment, *J. Mater. Chem. A*, 2014, **2**(29), 11490–11498.
- 25 L. Gu and et al, ., Bio-based polyurethanes with shape memory behavior at body temperature: Effect of different chain extenders, *RSC Adv.*, 2016, **6**(22), 17888–17895.
- 26 L. Botton and et al, ., Synthesis and properties of quick-drying UV-curable hyperbranched waterborne polyurethane coating, *Prog. Org. Coat.*, 2018, **125**, 201–206.
- 27 S. Kumar and et al, ., Biodegradable hybrid nanocomposite of chitosan/gelatin and green synthesized zinc oxide nanoparticles for food packaging, *Foods*, 2020, **9**(9), 1143.
- 28 S. S. Suryawanshi and et al, ., Bioconversion of sugarcane molasses into bioplastic (polyhydroxybutyrate) using *Bacillus cereus* 2156 under statistically optimized culture conditions, *Anal. Chem. Lett.*, 2020, **10**(1), 80–92.
- 29 S. Arasaretnam, Preparation of Biobased Plastic from Banana Peel and Application in Industrial Waste Water Purification, in *Conference Proceedings of the 2nd Asia International Conference on Multidisciplinary*, 2020.
- 30 L. Zhang and et al, ., Highly recoverable rosin-based shape memory polyurethanes, *J. Mater. Chem. A*, 2013, **1**(10), 3263–3267.
- 31 H.-M. Dou and et al, ., Bio-based, biodegradable and amorphous polyurethanes with shape memory behavior at body temperature, *RSC Adv.*, 2019, **9**(23), 13104–13111.
- 32 S. Shi and et al, ., Bio-based (co) polylactide-urethane networks with shape memory behavior at body temperature, *RSC Adv.*, 2016, **6**(83), 79268–79274.
- 33 N. T. Thanh, Study on effects of isocyanate on some properties of epoxy varnish, *J. Chem.*, 2022, **60**(1), 15–20.
- 34 N. Peamaroon, J. Jakmunee and N. Moonrungrsee, A Simple Colorimetric Procedure for the Determination of Iodine Value of Vegetable Oils Using a Smartphone Camera, *J. Anal. Test.*, 2021, **5**(4), 379–386.
- 35 Z. He and et al, ., Ultrasonication-assisted rapid determination of epoxide values in polymer mixtures containing epoxy resin, *Anal. Methods*, 2014, **6**(12), 4257–4261.
- 36 A. K. Bryan and et al, ., Measurement of mass, density, and volume during the cell cycle of yeast, *Proc. Natl. Acad. Sci. U. S. A.*, 2010, **107**(3), 999–1004.
- 37 M. Atif and et al, ., Effect of novel UV-curing approach on thermo-mechanical properties of colored epoxy composites in outsized dimensions, *J. Compos. Mater.*, 2016, **50**(22), 3147–3156.
- 38 H. Daud and et al, ., Preparation and characterization of guar gum based biopolymeric hydrogels for controlled release of antihypertensive drug, *Arabian J. Chem.*, 2021, **14**(5), 103111.
- 39 G. Kumar, L. Karthik and K. V. B. Rao, Hemolytic activity of Indian medicinal plants towards human erythrocytes: an *in vitro* study, *Elixir Applied Botany*, 2011, **40**(5534), e5537.
- 40 A. N.-A. Amr and et al, ., Anti-cancer and anti-oxidant activity of some Egyptian medicinal plants, *J. Med. Plants Res.*, 2009, **3**(10), 799–808.
- 41 A. Ramjan and et al, ., Evaluation of thrombolytic potential of three medicinal plants available in Bangladesh, as a potent source of thrombolytic compounds, *Avicenna J. Phytomed.*, 2014, **4**(6), 430–436.
- 42 B. Smith, The Infrared Spectra of Polymers V: Epoxies, *Spectroscopy*, 2022, **37**(3), 17–19.
- 43 Sigma-Aldrich, *IR Spectra Table and Chart*, 2022, available from, <https://www.sigmaaldrich.com/PK/en/technical-documents/technical-article/analytical-chemistry/photometry-and-reflectometry/ir-spectrum-table>.
- 44 M. Atif and et al, ., Electrochemical Evaluation of Human Hair Derived Carbon Particles, *ECS J. Solid State Sci. Technol.*, 2020, **9**(5), 051003.
- 45 P. Somdee and et al, ., Thermal analysis of polyurethane elastomers matrix with different chain extender contents for thermal conductive application, *J. Therm. Anal. Calorim.*, 2019, **138**(2), 1003–1010.
- 46 L. M. Leung and J. T. Koberstein, DSC annealing study of microphase separation and multiple endothermic behavior in polyether-based polyurethane block copolymers, *Macromolecules*, 1986, **19**(3), 706–713.
- 47 M. Ahmad and et al, ., Synthesis and characterization of polyurethane-based shape-memory polymers for tailored Tg around body temperature for medical applications, *Macromol. Chem. Phys.*, 2011, **212**(6), 592–602.
- 48 A. Kausar and A. Ur Rahman, Effect of graphene nanoplatelet addition on properties of thermo-responsive shape memory polyurethane-based nanocomposite, *Fullerenes, Nanotubes, Carbon Nanostruct.*, 2016, **24**(4), 235–242.

